Supplement of Clim. Past, 10, 955–973, 2014
http://www.clim-past.net/cp-10-955-2014/
doi:10.5194/cp-10-955-2014-supplement

Climate of the Past
Open Access

Supplement of

Orbitally tuned timescale and astronomical forcing in the middle Eocene to early Oligocene

T. Westerhold et al.

Correspondence to: T. Westerhold (twesterhold@marum.de)

Supplementary Document S1: Paleomagnetism of Site U1333

Introduction

The paleomagnetic data used to determine the magnetostratigraphy for Site U1333 (10.51655°N, 221.58072°E, Water Depth 4853 m) are provided as supplementary data tables. This document provides a guide to the data in the tables and additional information about the sampling, measurements, methods, and processing.

Background

The sampling strategy, measurement protocol, and magnetostratigraphic interpretation used in the present study was guided by results obtained during Expedition 320 by the shipboard paleomagnetism team (Gary Acton, Yuhji Yamamoto, Christian Ohneiser, Carl Richter, and Helen Evans). Results from that study are available in Pälike et al. (2010), which includes supplementary data tables with paleomagnetic measurements for all archive-half split-core sections and discrete paleomagnetic cube samples (~7 cm3). Vector demagnetization diagrams and principal component analysis (PCA) directions obtained from progressive thermal or alternating field (AF) demagnetization of discrete samples in that study provide constraints on magnetization acquisition and magnetic mineralogy pertinent to this study.

Sampling

Three holes (U1333A, B, and C) were cored at Site U1333 in ensure recovery of a complete stratigraphic section. A total of 531.65 m of core was recovered from 49 cores collected using the Advanced Piston Corer (APC) and 17 cores collected using the Extended Core Barrel (XCB) coring system. The XCB cores were not sampled for paleomagnetic analysis in this study because it is not possible to azimuthally reorient the cores, and therefore the paleomagnetic declination is indeterminate. Given the low paleolatitude of Site U1333, the

paleomagnetic inclination is also too shallow to confidently determine the magnetic polarity from inclination data along. Thus, we sampled only APC cores.

A total of 88 U-channel samples (2 cm x 2 cm x 150 cm) were collected continuously along the spliced composite stratigraphic section from 96 to 190 adjusted revised meters composite depth (rmcd). The stratigraphic splice and rmcd scale are provided in Westerhold et al. (2012).

Measurements

Measurements were made in the Paleomagnetism Laboratory at the University of California–Davis using a 2G Enterprises long-core cryogenic magnetometer (Model 755), which resides within a magnetically shielded room. Each U-channel sample was subjected to progressive AF demagnetization from 0 mT up to 80 or 100 mT typically in 8 to 11 steps and the magnetic remanence was measured every 1 cm following each demagnetization step. Raw inclination, declination, and intensity data for each measurement step is provided in Supplementary Tables S17-19.

Processing

Paleomagnetic directions were determined from principal component analysis (PCA) (Kirschvink, 1980), in which remanence measurements from at least five demagnetization steps for each interval were fit to lines. Only steps between 20 and 60 mT were used. Program Zplotit (Acton, 2011, http://paleomag.ucdavis.edu/software-zplotit.html) was used to search iteratively for the best-fit line segments, determine PCA directions, and produce vector demagnetization diagrams, intensity-decay plots, and stereonets. Lines were fit using both the FREE option of PCA, in which the line is not required to pass through the origin of the plot, and the ANCHORED option of PCA, in which line is anchored to the origin (Supplementary Tables S17-S19). In addition, a Fisherian mean direction was computed from the highest several demagnetization steps used in the PCA. This Fisherian direction is referred to as a stable end point (SEP). Comparison between the FREE PCA, ANCHORED PCA, and SEP can be used to assess the stability of the characteristic remanent magnetization (ChRM) and the presence of unremoved magnetic overprints. The FREE PCA direction is used as the preferred direction in the magnetostratigraphic interpretation.

Correlation of the ~180° alternations in the composite paleomagnetic declination record with the geomagnetic polarity timescale (GPTS) provides the basis for the magnetostratigraphic interpretation. To construct this record, the declination at the base of the first core collected is matched to the declination from another core from a different hole that contains a coeval interval, and then this process in repeated down the stratigraphic section. This strategy is possible because coring in the three holes is conducted such that there is stratigraphic overlap between cores from the different holes, ensuring that a complete stratigraphic section is obtained. For aesthetic purposes, the declination for each core has been rotated by a constant amount such that the average declination for normal and reversed polarity intervals are approximately 0° and 180°, respectively. Because the Pacific Plate has not rotated much since the Eocene, this also gives declinations that are close to true values. In addition, APC cores sometimes have a small within-core azimuthal rotation, which occurs as the piston corer penetrates the sediments. These tend to produce subtle sigmoidal variations in declination within a core, which are too small to influence the magnetostratigraphic interpretation but that are a bias unrelated to the geomagnetic field. This artifact has been removed by fitting a sigmoid to the declination-vs.-depth data for each core and then subtracting that value from the observed value, in a manner similar to that described by Lanci et al. (2004).

Paleomagnetic Results

As shown in Pälike et al. (2010), the Site U1333 sediments are accurate recorders of the paleomagnetic field. Generally, AF demagnetization up to 10 to 20 mT was sufficient to remove drilling-related overprints and resolve the ChRM component in the split-core samples.

Our more detailed AF demagnetization results provide confirmation of the stability of the ChRM, while also resolving it more accurately and precisely. Line fits through the demagnetization data using PCA (FREE fitting option) were well constrained, with average maximum angular deviation (MAD) angles of 2.3° for the 10,896 intervals used in the magnetostratigraphic interpretation (Supplementary Figure S13 and S14 and Tables S17-S19). The linear decay of magnetization is generally to the origin of the vector demagnetization diagrams, as illustrated in Supplementary Figure S15a and S15b for a sequence of samples across the Chron C13n/C13r boundary. This sequence shows that the paleomagnetic direction can be very well resolved even for samples only a few centimeters on either side of the reversal boundary (e.g., the reversed polarity sample in Supplementary Figure S15E is only 3 cm below the Chron C13n/C13r reversal and the normal polarity sample in Supplementary

Figure S15C is only 2 cm above the reversal. Only the sample in the very middle of the reversal (Supplementary Figure S15D) has a poorly defined direction and large MAD angle, which is not unexpected because during reversals the geomagnetic field is much more weak and variable in direction than during stable polarity intervals.

Even though most samples have magnetizations that decay to the origin of vector demagnetization diagrams, some samples decay to positions near rather than directly to the origin. We observed that most of those samples that do not decay directly to the origin were from cores that were collected with a standard metal bottom-hole assembly (BHA) and core barrel whereas those samples that decay directly to the origin were collected with a non-magnetic BHA and non-magnetic core barrel. U-channel samples that included more material from the periphery of the core also had stronger drilling overprints. Sampling the core periphery occurs when the split-core section is relatively thin (≤ 2 cm). In either case, the minor overprint does not affect the declinations appreciably and, hence, has no impact on the magnetostratigraphic interpretation.

The downhole variation in the ChRM direction is one with fairly consistent shallow inclination, as expected for sediments deposited near the paleo-equator, and with declinations that alternate between two stable states that are antipodal, representing normal and reverse polarity magnetozones (Figure S14). The zonation can readily be correlated to the GPTS, a process that is facilitated by biostratigraphic constraints. Given these properties, it is clear the ChRM is a primary depositional remanent magnetization that records the reversals of the geomagnetic field.

Based on the results of AF demagnetization results from the U-channels, thermal demagnetization results conducted on discrete samples during Expedition 320, and a myriad of other rock magnetic measurements conducted on equatorial Pacific sediments from Site U1333 and nearby drill sites (e.g., Lanci et al., 2004 and 2005; Pares and Lanci, 2004; Guidry et al., 2013; Ohneiser et al., 2013; Yamamoto et al., 2013; Yamazaki et al., 2013), the ChRM is carried primarily by biogenic magnetite and detrital titanomagnetite and/or titanomaghemite.

Magnetostratigraphic Interpretation

The revised magnetostratigraphy is derived from the distinct ~180° alternations in magnetic declination that occur along the composite stratigraphic section (Supplementary Figure S14 and Tables S17-S19). Correlation of these with the GPTS illustrates that the magnetozones

from 96 to 190 rmcd correspond to chronozones spanning from the middle of Chron C11r to within Chron C20n (Figure S14 and Table 1).

This magnetostratigraphic interpretation is basically the same as that given in Pälike et al. (2010), although the locations of the reversals have been refined. The oldest reversal observed by Pälike et al. (2010) was the base of Chron C20n, which occurred near the bottom of the last APC core collected in Hole U1333C. In this study, we interpret only down to the top of Magnetozone C20n. Of the 23 reversals that occur between the base of Magnetozone C11r and top of Magnetozone C20n, the difference between Pälike et al. (2010) and the revised depth estimates is <5 cm for 11 reversals and <20 cm for all but 3 of the remain 12 reversals. The largest change, 163 cm, is for the depth of the reversal associated with the Chron C12r/C13n boundary. For Hole U1333C, this could only be constrained to occur between Cores U1333C-13H and -14H in the split-core data but could be constrained to occur at about 47 cm from the top of Core U1333C-14H in the U-channel data.

Ages

We use the ages from the astronomically tuned age model for Site U1333 from this paper (Supplementary Table S15). The age model encompasses all sediments deposited from the base of Chron C12n to the top of Chron C20n. The paleomagnetic data extend through that entire interval and a few meters up section through sediments that were deposited during Chron C11r. For these younger sediments, we use the ages from Pälike et al. (2006).

Paleomagnetic Data Tables

The following is a description of the paleomagnetic data provided in Tables S17-S19:

U-channel Sample: The naming convention follows that from IODP. For example, sample U1333A-10H-1 is a U-channel collected along Section 1 of Core 10H from Hole U1333A.

Interval: The interval along the U-channel measured from the top.

Depths:

mbsf = meters below seafloor = CSF-A
mcd = meters composite depth = CCSF-A
amcd = adjusted mcd = rmcd = revised adjusted CCSF-A

Age: The ages are from this paper for the interval from Chron C12n (o) to C20n (y). Ages from Pälike et al. (2010) are used for younger chrons.

Half: Working (W) or Archive (A) half of the split-core sections.

Filter 1: This column is for culling data. It contains a 0 if the interval is considered biased or a 1 if the data are considered valid. Data are considered biased if they fall within disturbed intervals identified during sampling or based on core descriptions made on Expedition 320 (Pälike et al., 2010)

Filter 2: This column is for further culling data. Filter 2 is like Filter 1, but it also eliminates data within 4 cm of the ends of the U-channel samples, which often are biased by sample edge effects. This filter was used for the data in the magnetostratigraphic interpretation.

Raw Data: Columns with the prefix AFD, Dec, Inc, and Int followed by three numbers are the AF demagnetization step (mT), declination, inclination, and intensity (A/m). The three numbers give the demagnetization step. Hence AFD030, Dec030, Inc030, and Int030 are the data for the 30 mT demagnetization step.

PCA: Principal component analysis for FREE and ANCHORED lines, from program Zplotit (Acton, 2011, http://paleomag.ucdavis.edu/software-zplotit.html).

Declination Corrected for Constant & Within-Core Rotation: The preferred declination, which is the declination determined from the FREE PCA option corrected for azimuthal rotation of the core and for minor within core rotation as described above.

Polarity: N for normal, R for reversed, and X for disturbed or indeterminate intervals.

Chron: The polarity chron name. An X is put in the column for disturbed intervals.

Supplementary Material - Figures

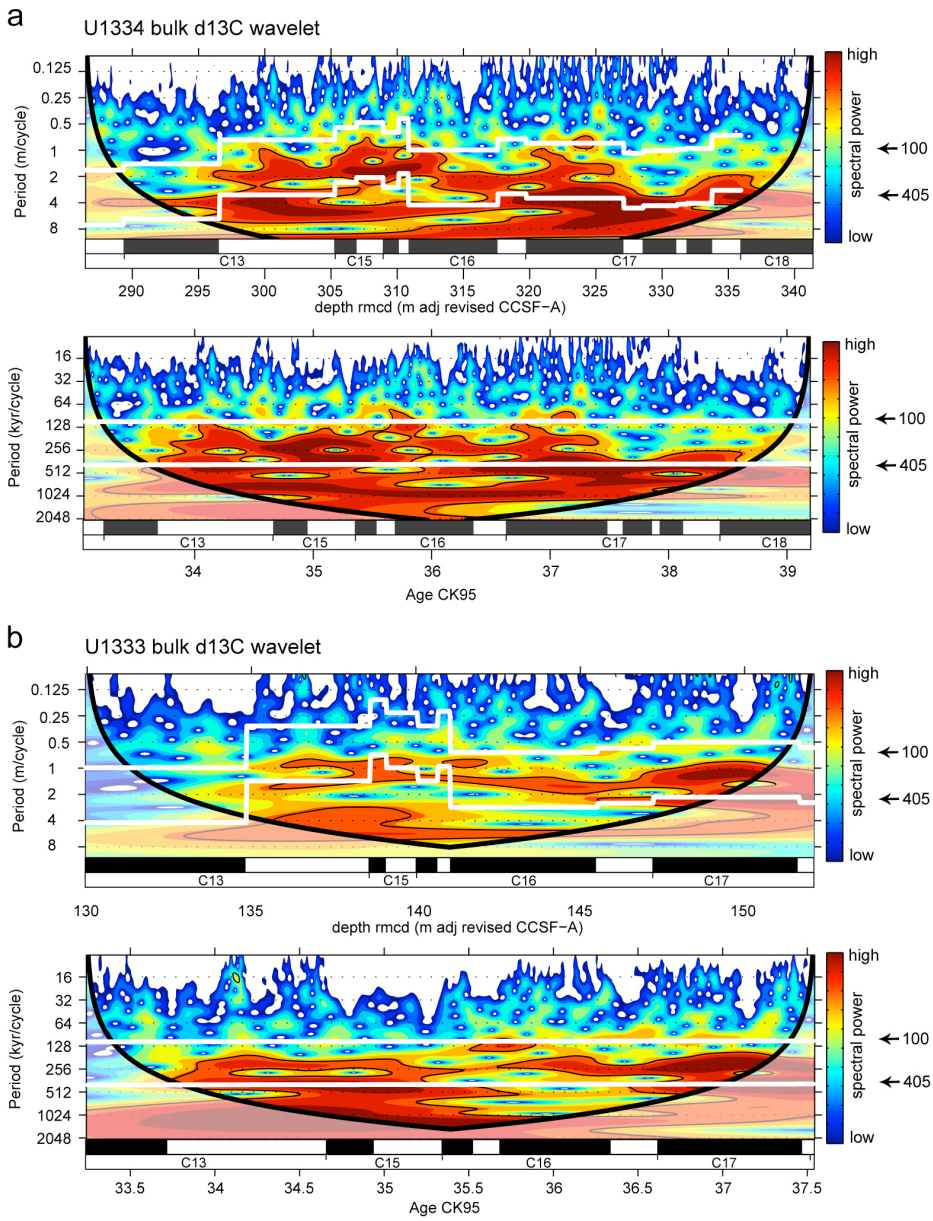

Figure S1. Evolutionary wavelet power spectra of bulk stable carbon isotope data from Site U1334 (a) and U1333 (b) for magnetochrons C13 to C18n.1n in the depth domain and versus age. The age model is based on magnetostratigraphy using the Time Scale of Cande and Kent (1995, CK95). The shaded contours in the evolutionary wavelet power spectra are normalized linear variances with blue representing low spectral power, and red representing high spectral power. The black contour lines enclose regions with more than 95% confidence. Shaded regions on either end indicate the cone of influence where edge effects become important. Distinct bands that run across the spectra indicate the dominance of Milankovitch frequencies. Thick white lines are the projected 100 and 405-kyr cycle path, respectively.

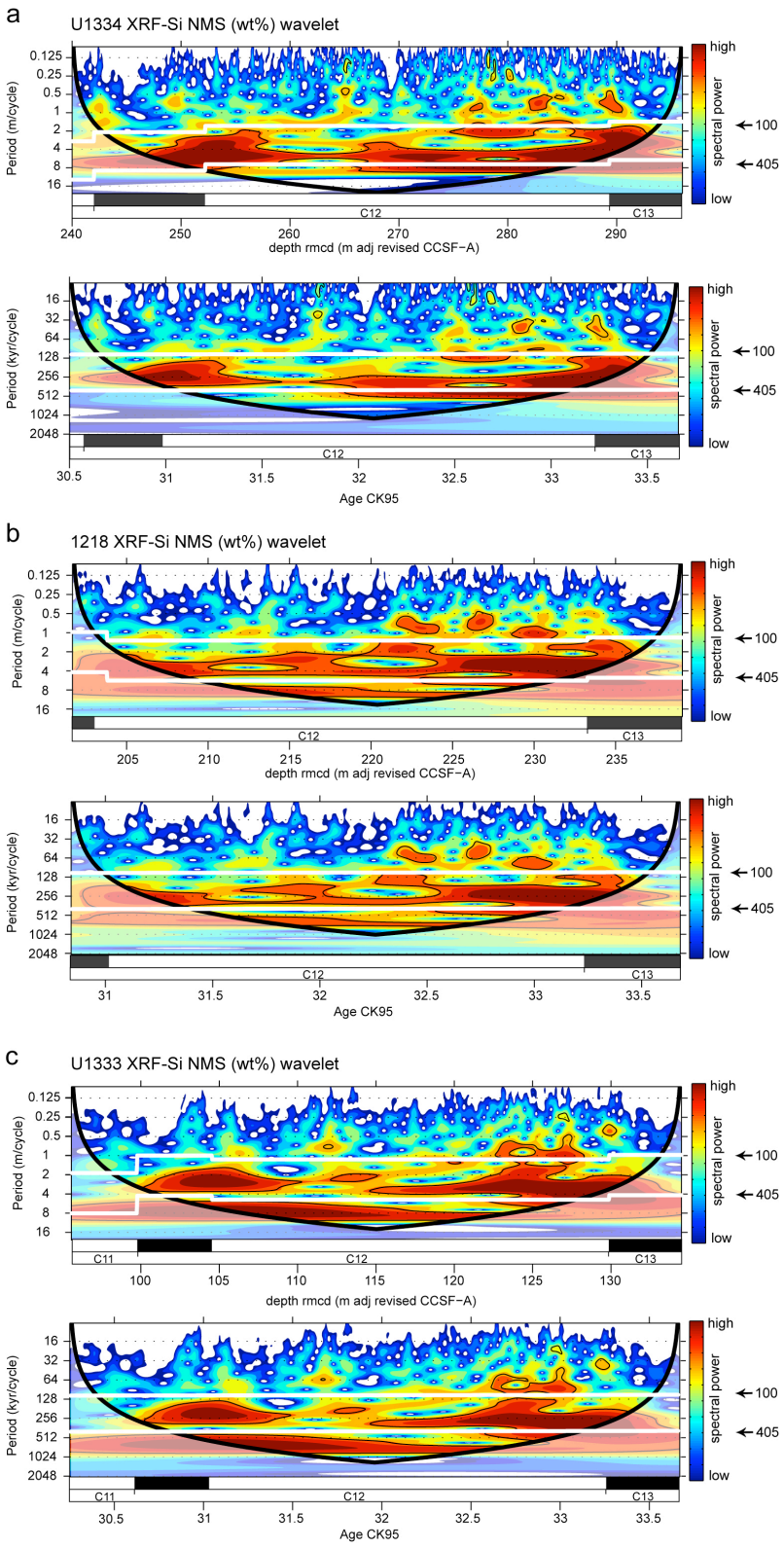

Figure S2. Evolutionary wavelet power spectra of XRF core scanning Normalized Median Scaled (NMS) Si intensity data expressed as SiO_2 wt% data from Site U1334 (a), 1218 (b) and U1333 (c) for the Oligocene magnetochrons C12n to C13n in the depth domain and versus age. For further explanation see Figure S1 text.

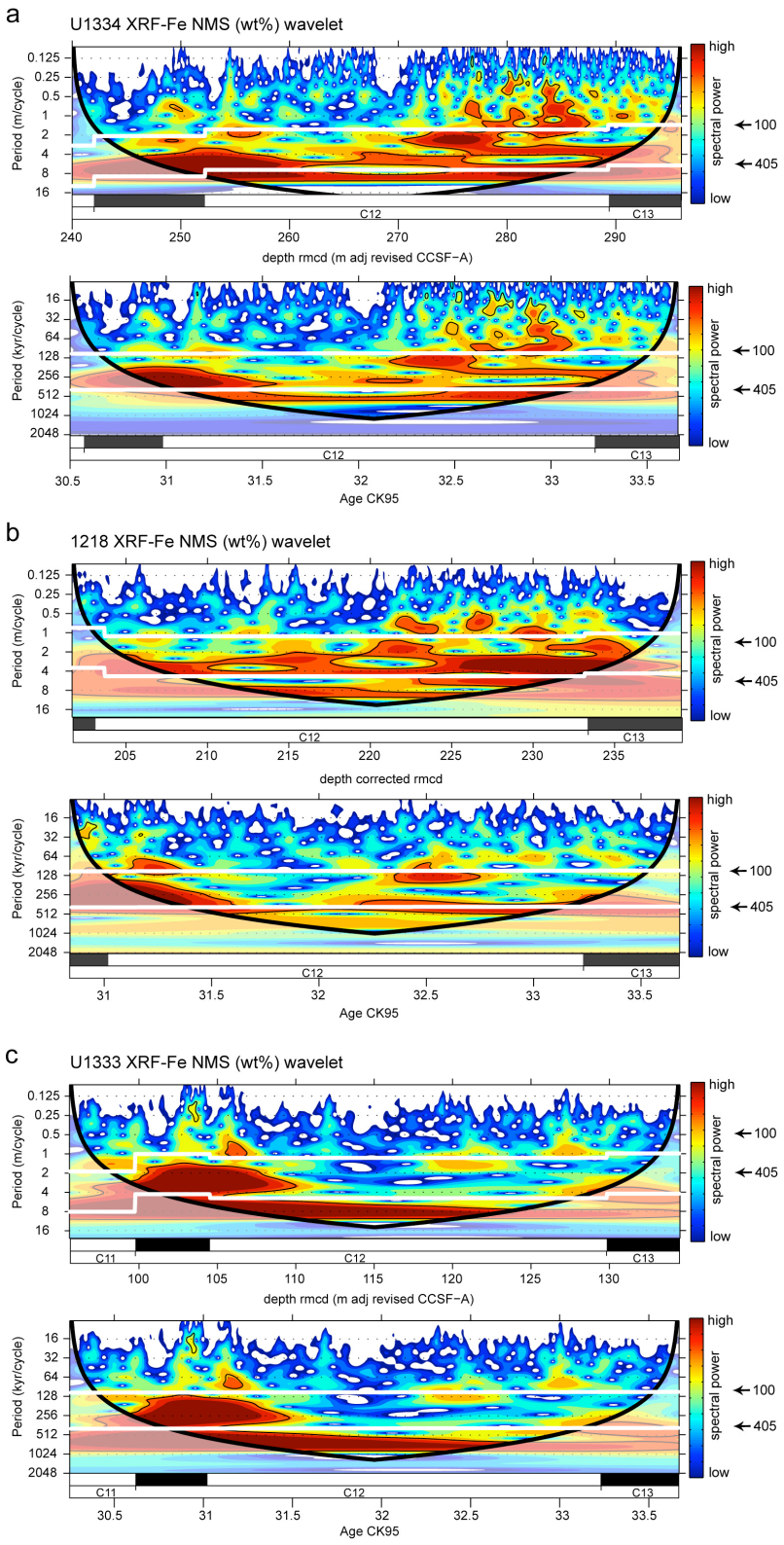

Figure S3. Evolutionary wavelet power spectra of XRF core scanning Normalized Median Scaled (NMS) Fe intensity data expressed as Fe_2O_3 wt% data from Site U1334 (a), 1218 (b) and U1333 (c) for the Oligocene magnetochrons C12n to C13n in the depth domain and versus age. For further explanation see Figure S1 text.

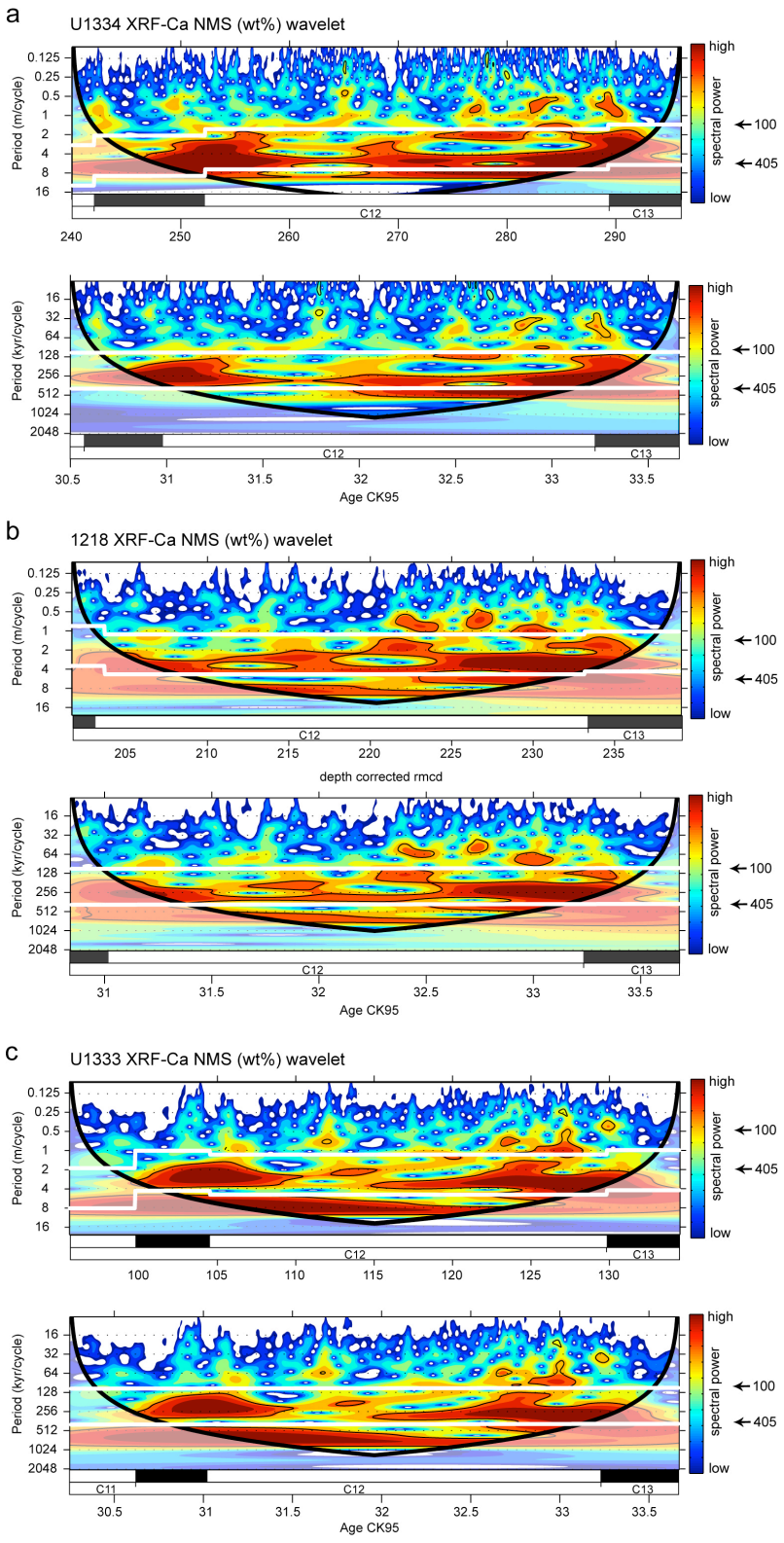

Figure S4. Evolutionary wavelet power spectra of XRF core scanning Normalized Median Scaled (NMS) Ca intensity data expressed as $CaCO_3$ wt% from Site U1334 (a), 1218 (b) and U1333 (c) for the Oligocene magnetochrons C12n to C13n in the depth domain and versus age. For further explanation see Figure S1 text.

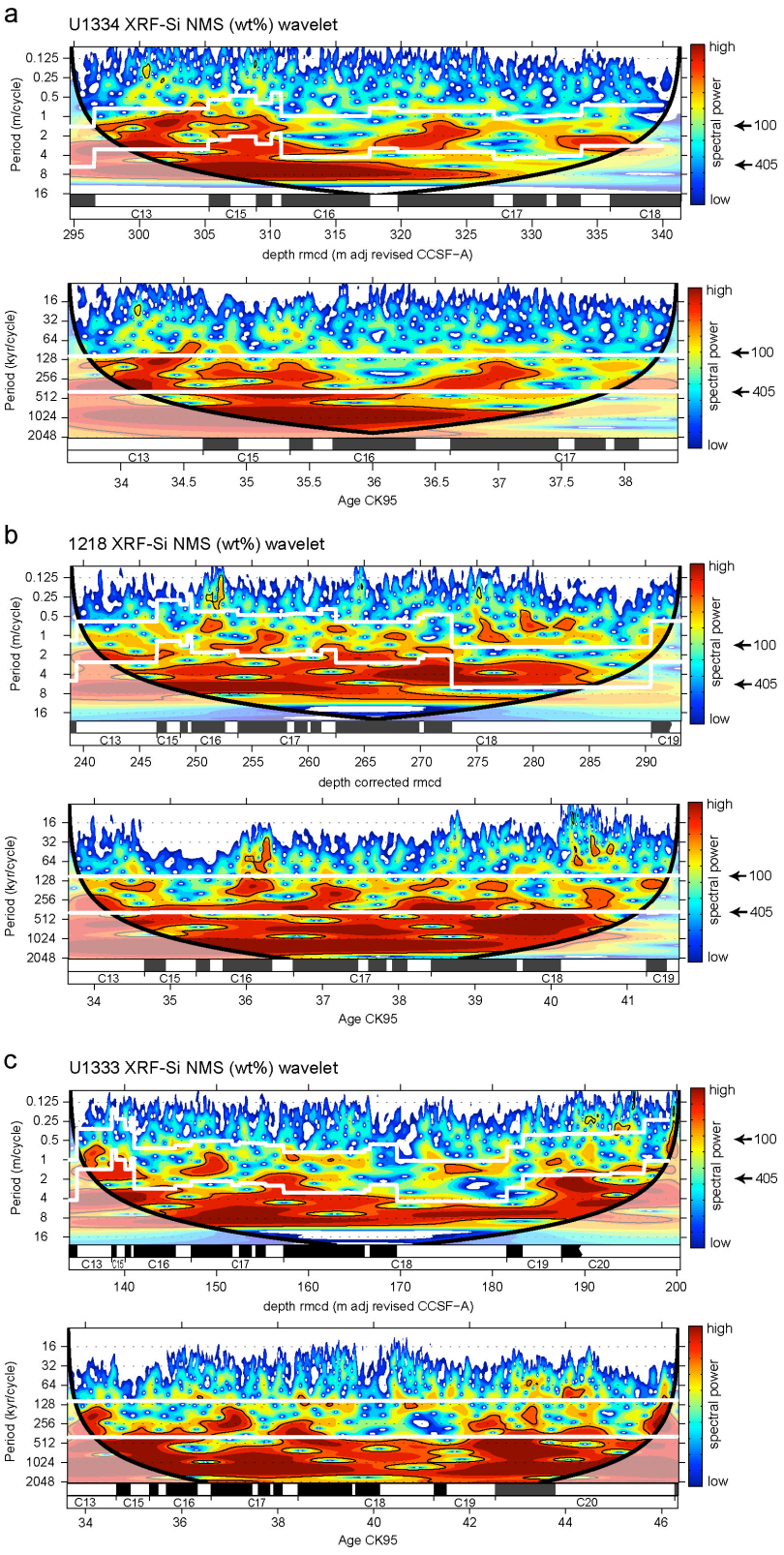

Figure S5. Evolutionary wavelet power spectra of XRF core scanning Normalized Median Scaled (NMS) Si intensity data expressed as SiO_2 wt% data from Site U1334 (a), 1218 (b) and U1333 (c) for the Eocene magnetochrons C13r to C20r in the depth domain and versus age. For further explanation see Figure S1 text.

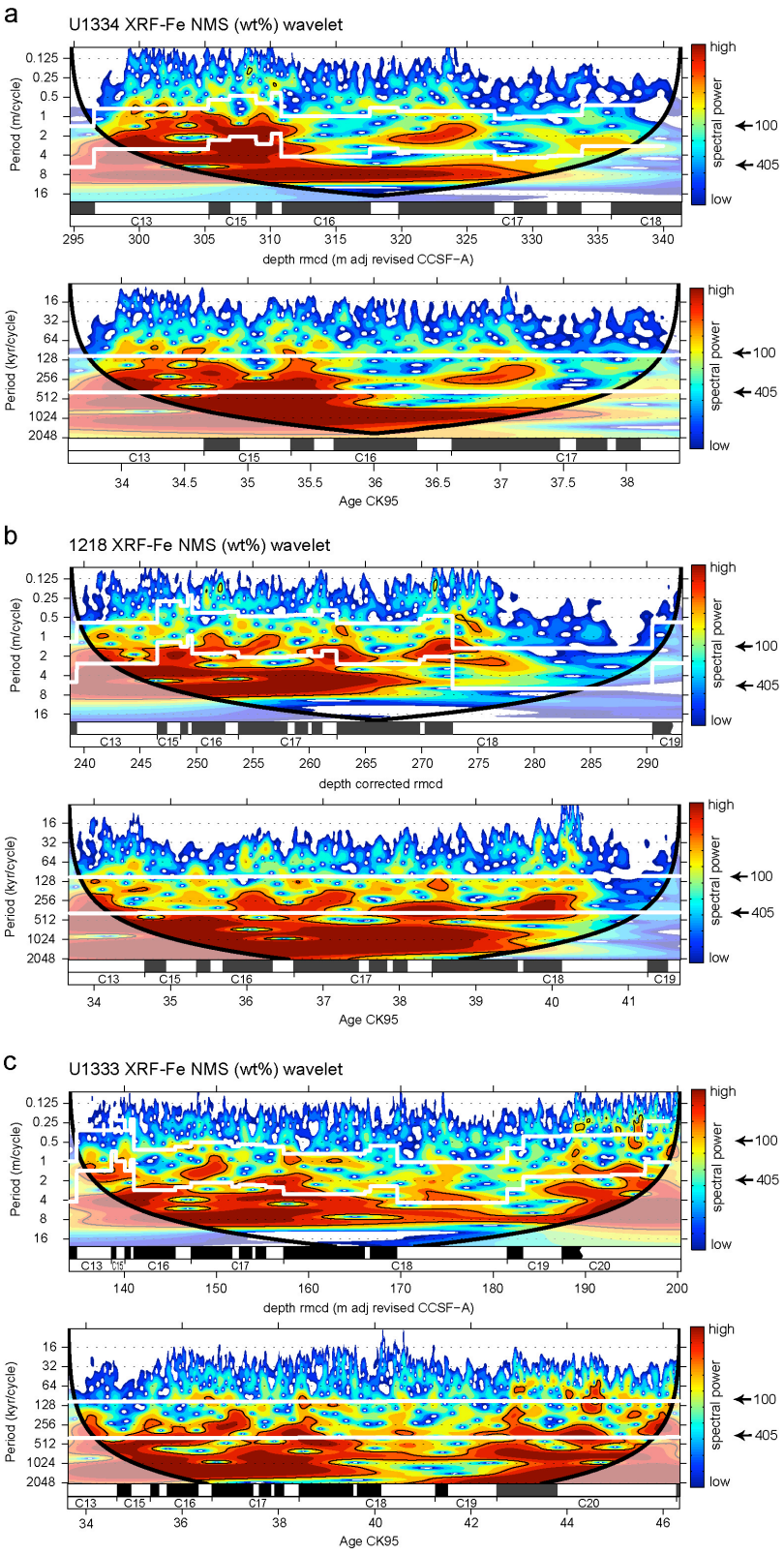

Figure S6. Evolutionary wavelet power spectra of XRF core scanning Normalized Median Scaled (NMS) Fe intensity data expressed as Fe_2O_3 wt% data from Site U1334 (a), 1218 (b) and U1333 (c) for the Eocene magnetochrons C13r to C20r in the depth domain and versus age. For further explanation see Figure S1 text.

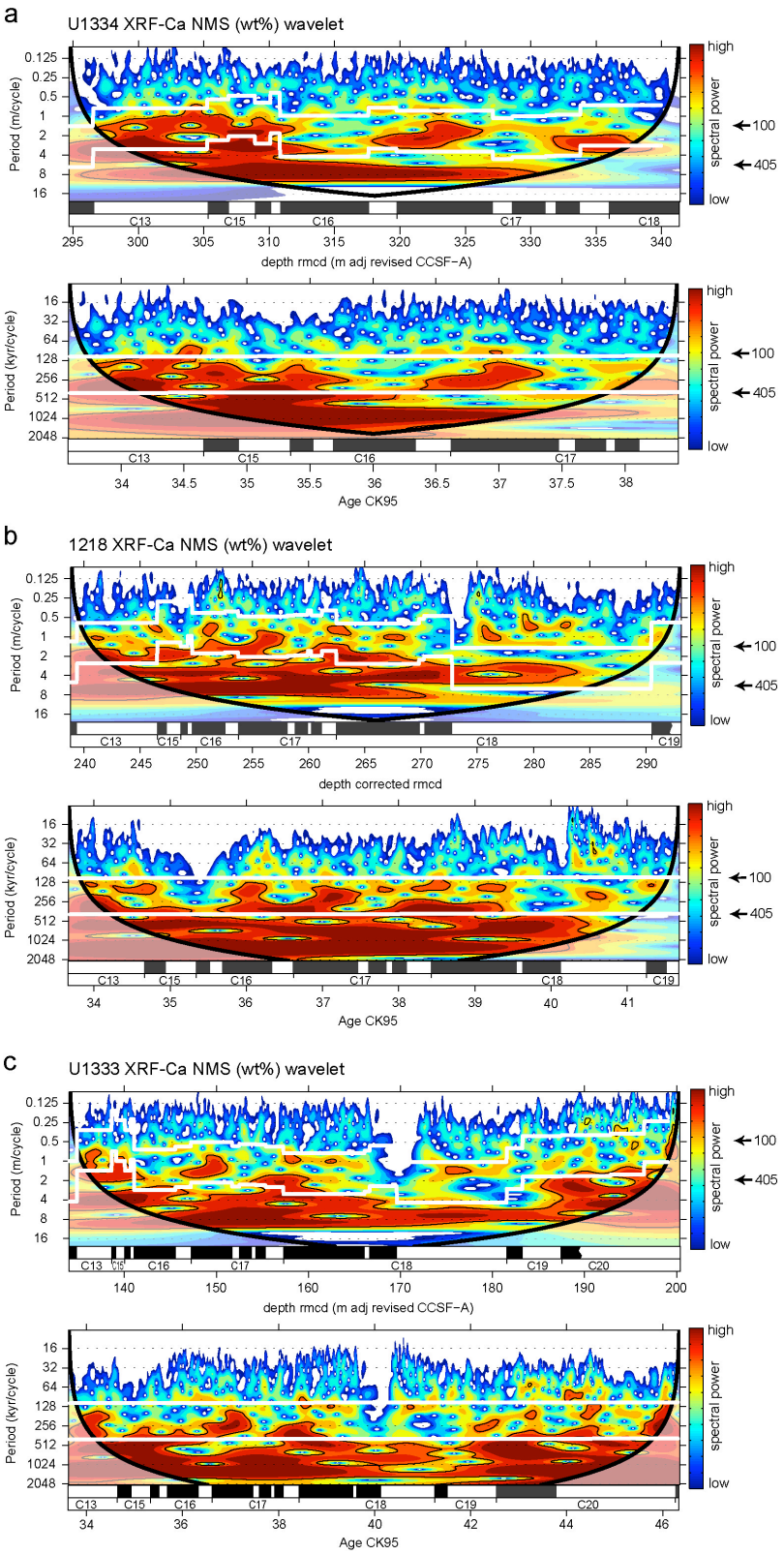

Figure S7. Evolutionary wavelet power spectra of XRF core scanning Normalized Median Scaled (NMS) Ca intensity data expressed as $CaCO_3$ wt% from Site U1334 (a), 1218 (b) and U1333 (c) for the Eocene magnetochrons C13r to C20r in the depth domain and versus age. For further explanation see Figure S1 text.

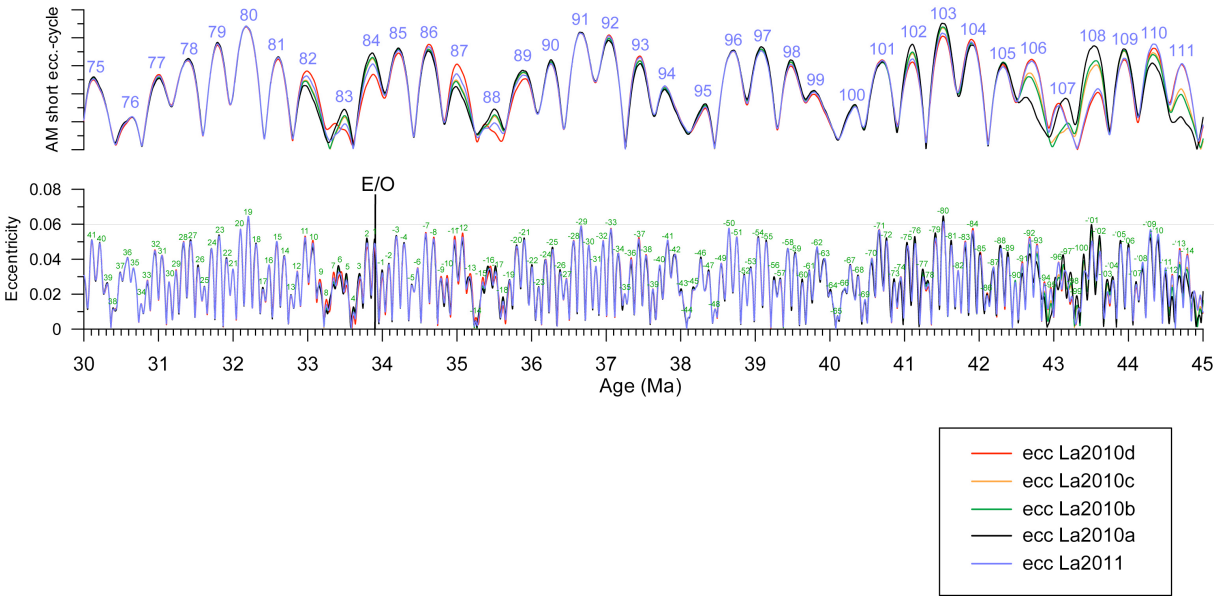

Figure S8. Short (100 kyr) and long (405 kyr) eccentricity cycle number definition for the astronomical solutions from 30 to 45 Ma as used in this publication. Lower panel shows earth's orbital solution for eccentricity from Laskar et al. (2011a, four solutions a to d) and Laskar et al. (2011b). Each short eccentricity is labeled with a number (green) counting from the in this paper established position of the Eocene/Oligocene boundary. This facilitates comparing the cycle extracted from the geological data to the orbital solution. The upper panel shows the amplitude modulations extracted with the program ENVELOPE (Schulz et al., 1999) of the short eccentricity cycle. For details about the solutions and their stability over time see the discussion in Westerhold et al. (2012b).

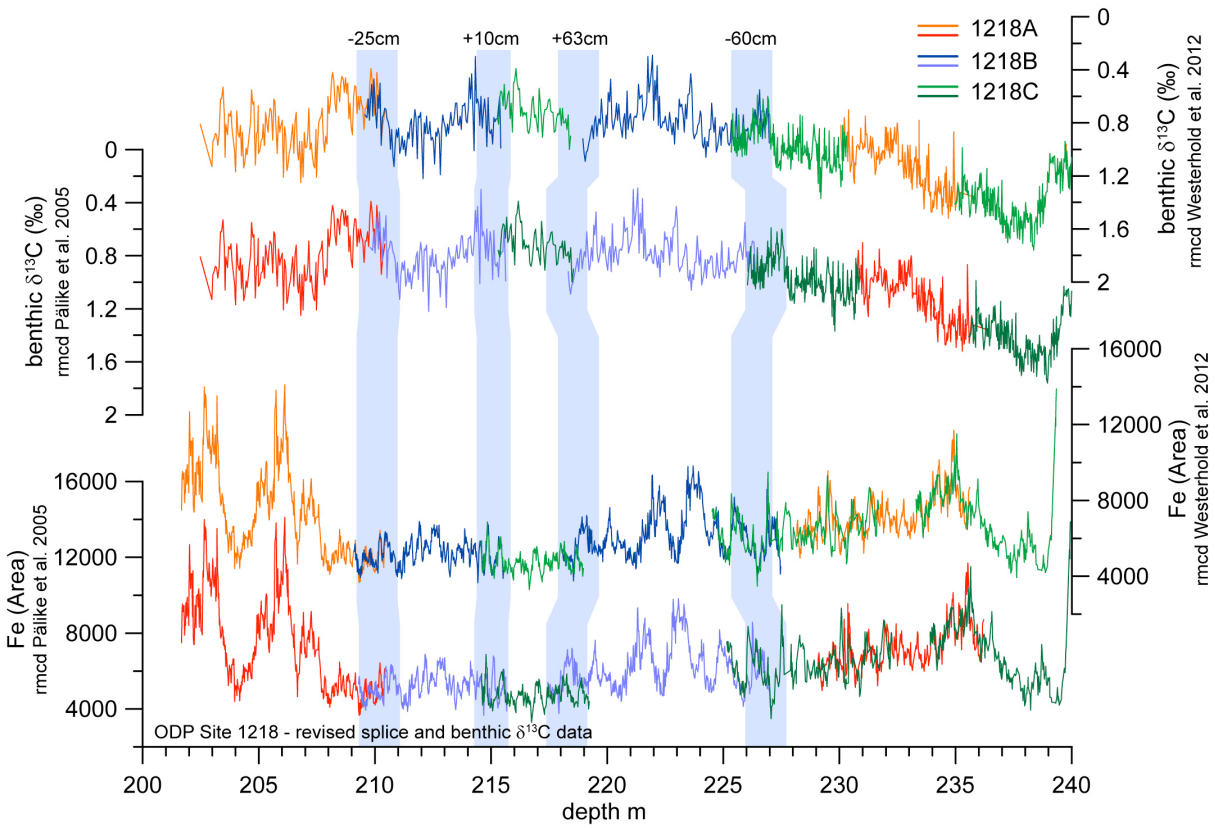

Figure S9. XRF core scanning Fe (Iron) intensity data (this study) and benthic $\delta^{13}C$ data from ODP Site 1218 (Coxall et al., 2005; Wade and Pälike, 2004; Pälike et al., 2006; Coxall and Wilson, 2011) plotted on the rmcd of Pälike et al. (2005) and the corrected rmcd of Westerhold et al. (2012a) to illustrate changes in the composite record. Data are plotted for holes 1218A (red), 1218B (blue) and 1218C (green) separately to highlight overlaps, gaps and mismatches. The blue bars mark changes in the composite record including the amount of change in cm. As an example, the change around 227 m illustrates that the splice of Pälike et al. (2005) doubled a prominent $\delta^{13}C$ decrease (one full 100-kyr eccentricity cycle) and therefore retuning of this interval was required.

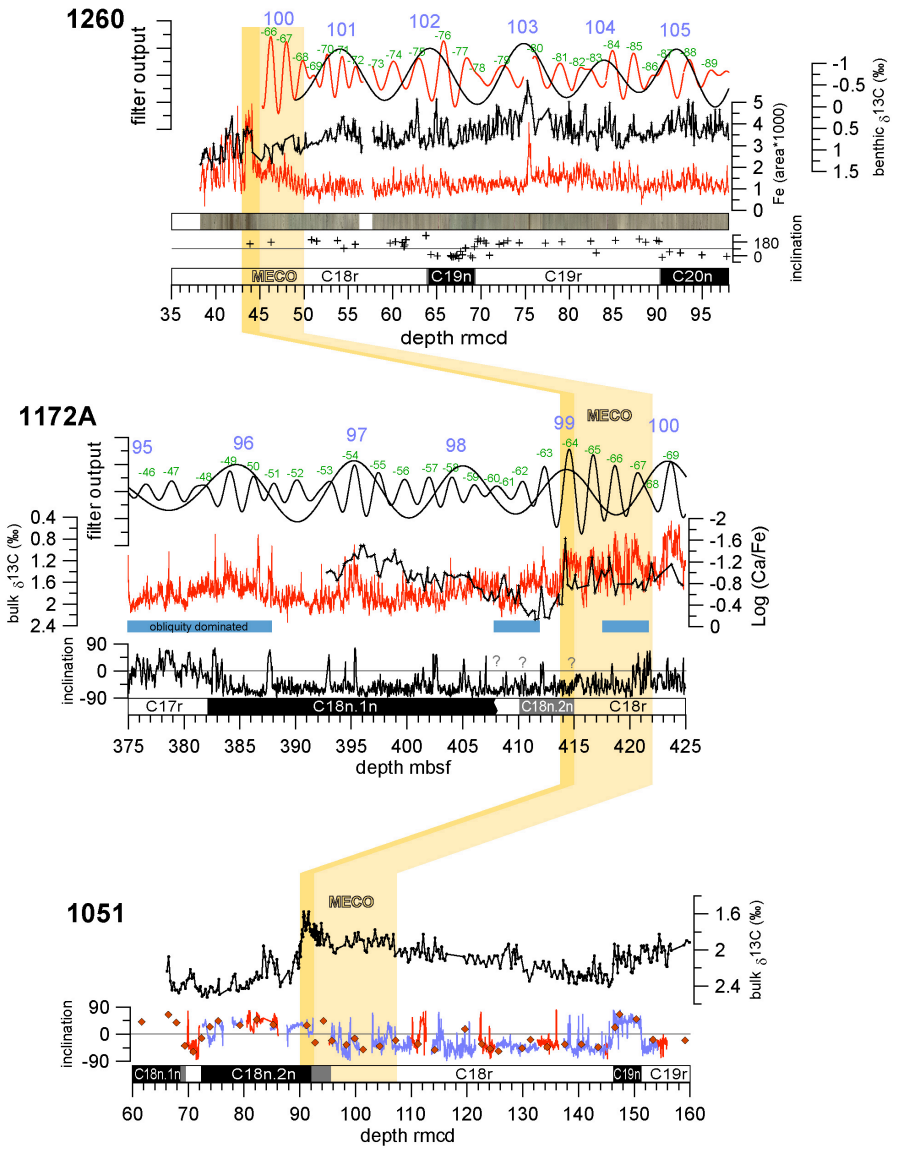

Figure S10. Correlation of the Middle Eocene Climate Optimum (MECO) between ODP Sites 1260 (Demerara Rise), 1172A (East Tasman Plateau) and 1051 (Blake Nose). For detailed caption of 1260 and 1172A data see Figure 7. Additional data: inclination data from discrete samples for 1260 (black crosses; Suganuma and Ogg, 2006; Edgar et al., 2007); for 1172A shipboard inclination data (black line; Shipboard Scientific Party, 2001) and the bulk stable carbon isotope data (Bijl et al., 2010). Data from 1051: Magnetostratigraphy and u-channel inclination data (1051A – red, 1051B – blue; Edgar et al. 2010), inclination from discrete samples (red diamonds; Suganuma and Ogg, 2006), bulk stable carbon isotope data (black line with dots; Bohaty et al., 2009). The darker orange correlation band marks the carbon isotopes excursion (CIE) of the peak-MECO.

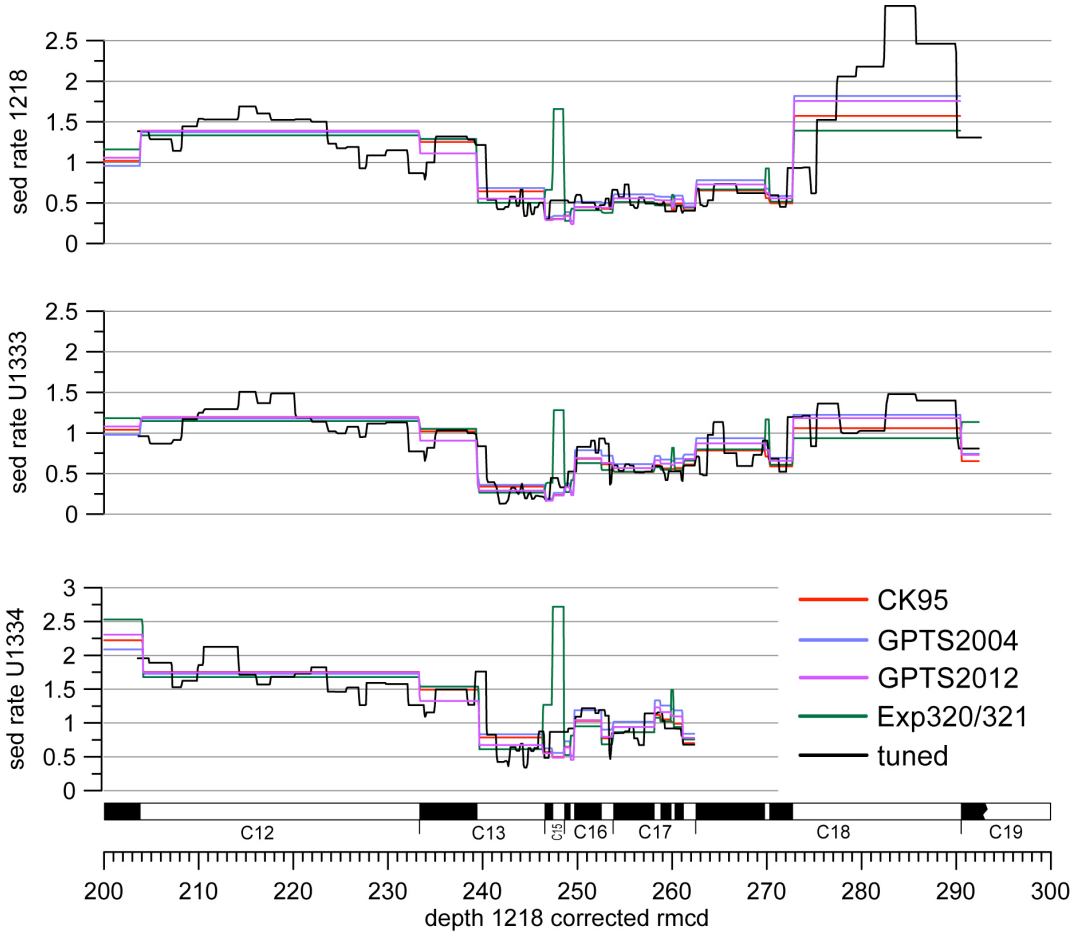

Figure S11. Sedimentation rate plots for Sites 1218, U1333 and U1334 based on magnetostratigraphy and different ages for magnetochron boundaries mapped onto 1218 corrected rmcd. CK95 - Cande and Kent 1995; GPTS2004 – Geomagnetic Polarity Time Scale 2004 - Ogg and Smith (2004); GPTS2012 – Ogg (2012); Exp320/321 – Pälike et al. (2010) based on Pälike et al. (2006); tuned – this paper.

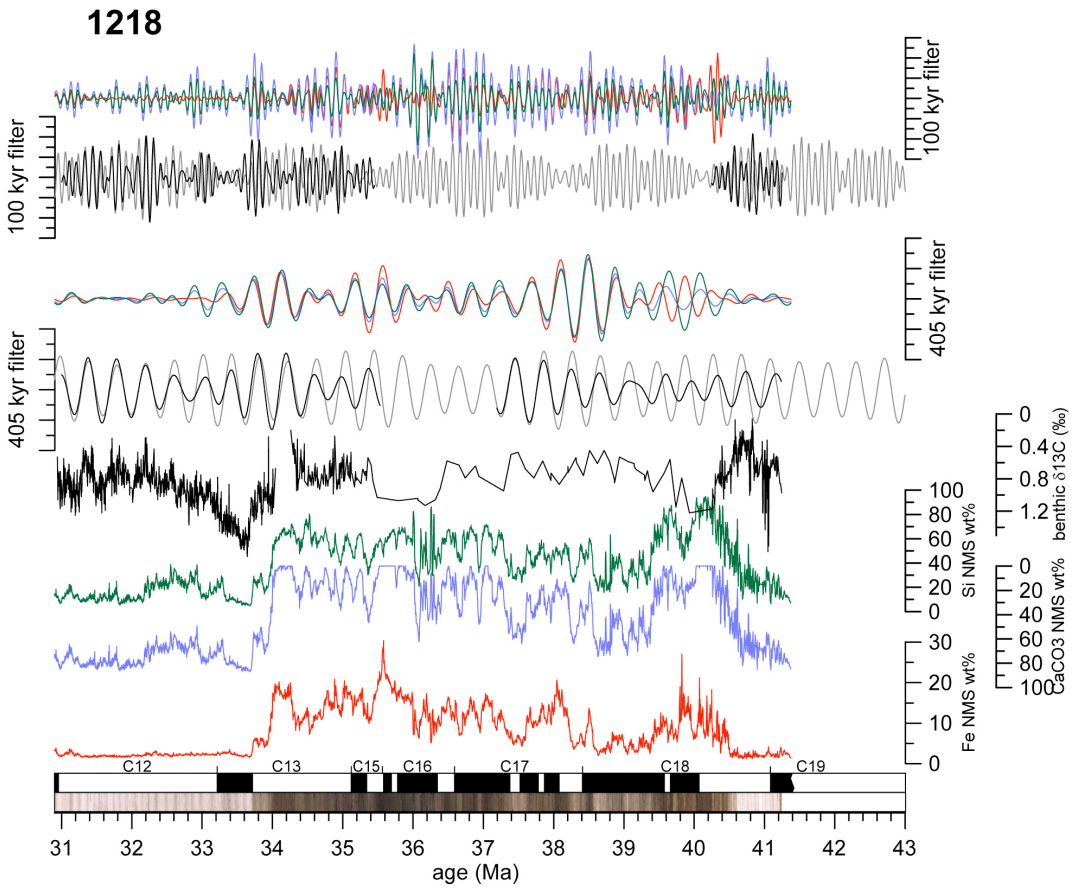
1218
100 kyr filter
405 kyr filter
benthic δ13C (‰)
Si NMS wt%
CaCO3 NMS wt%
Fe NMS wt%
C12
C13
C15
C16
C17
C18
C19
age (Ma)

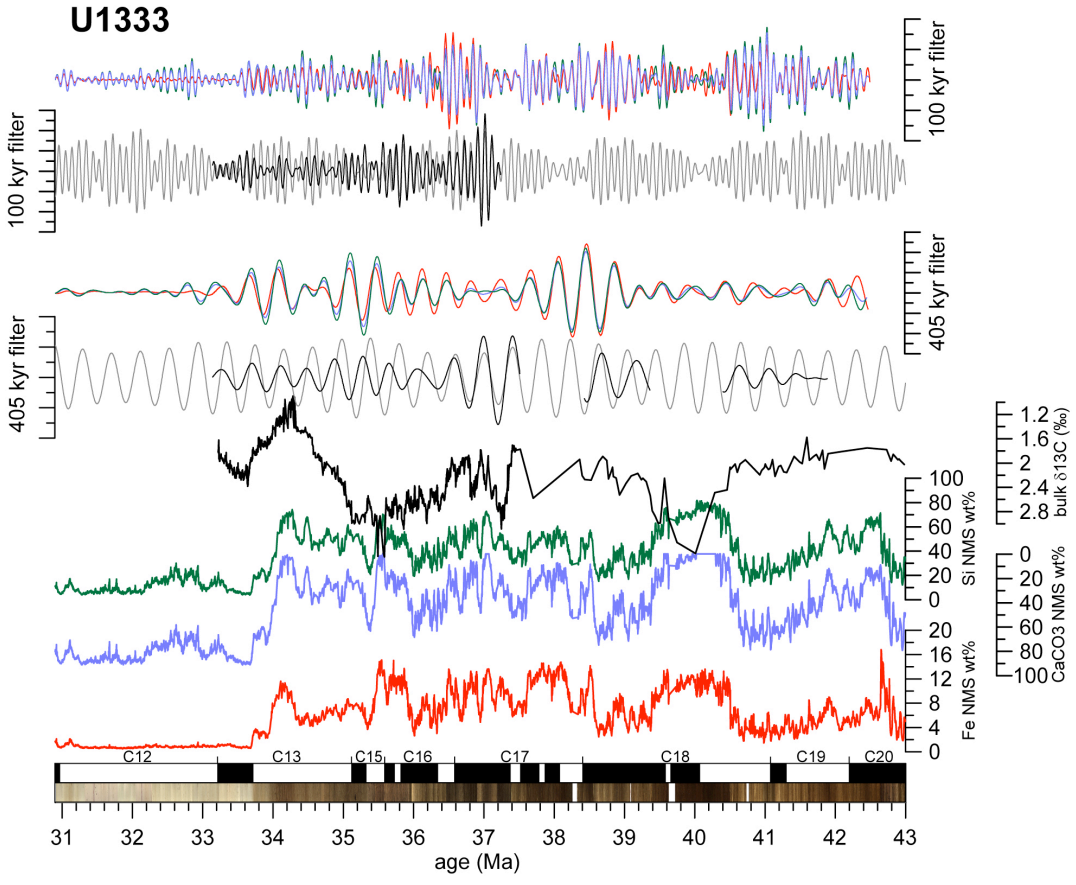
U1333
100 kyr filter
405 kyr filter
bulk δ13C (‰)
Si NMS wt%
CaCO3 NMS wt%
Fe NMS wt%
C12
C13
C15
C16
C17
C18
C19
C20
age (Ma)

Figure S12 a & b. Calibrated XRF Fe (red), Ca (blue), and Si (green) core scanning data, stable isotope data (black) and band pass filters plotted on the tuned age model for sites 1218 (a) and U1333 (b). Grey curve is the 100 (0.1 ± 0.03 cycles/kyr) and 405 (0.02469 ± 0.007) kyr filter of the La2011 (Laskar et al. 2011) orbital solution. Filters for data are only given at intervals where the resolution is high enough to resolve the cyclicity.

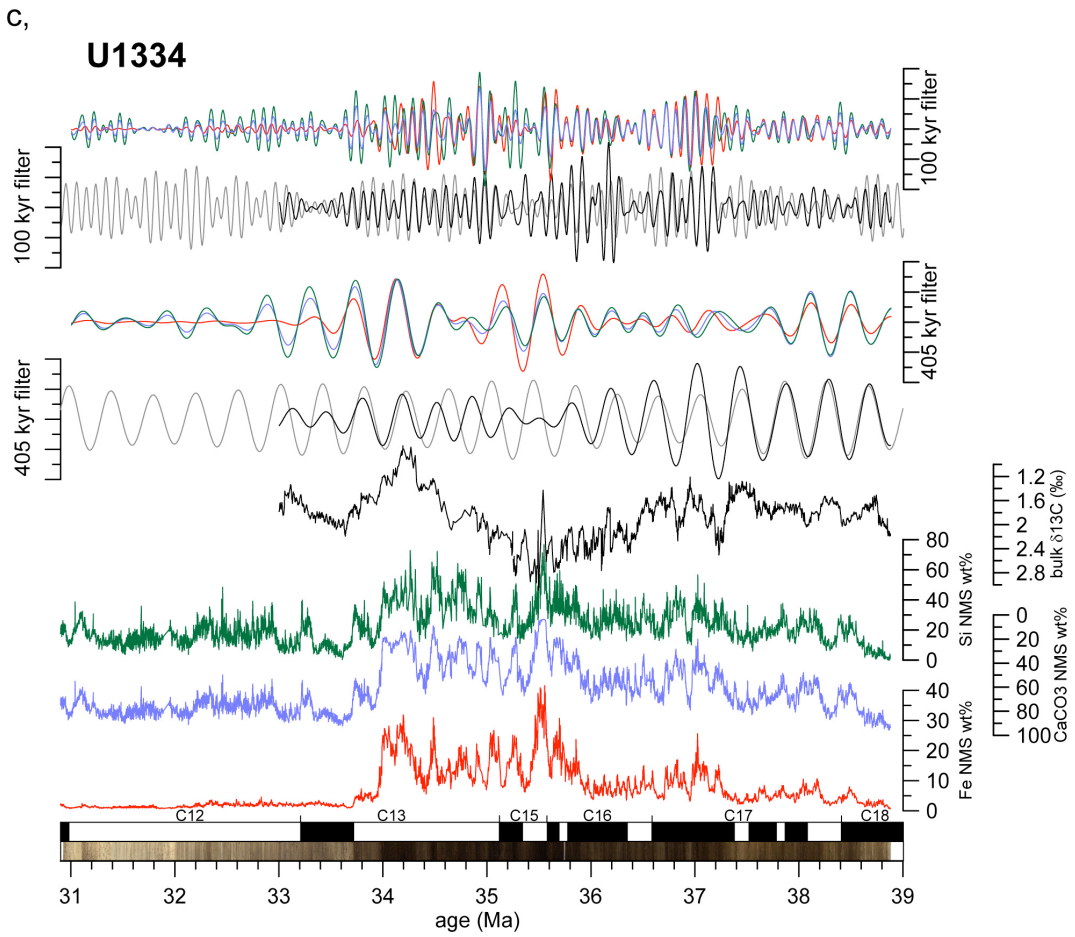

Figure S12 c. Calibrated XRF core scanning data, stable isotope data and band pass filters plotted on the tuned age model for Site U1334. For further reference see Fig. S12a&b.

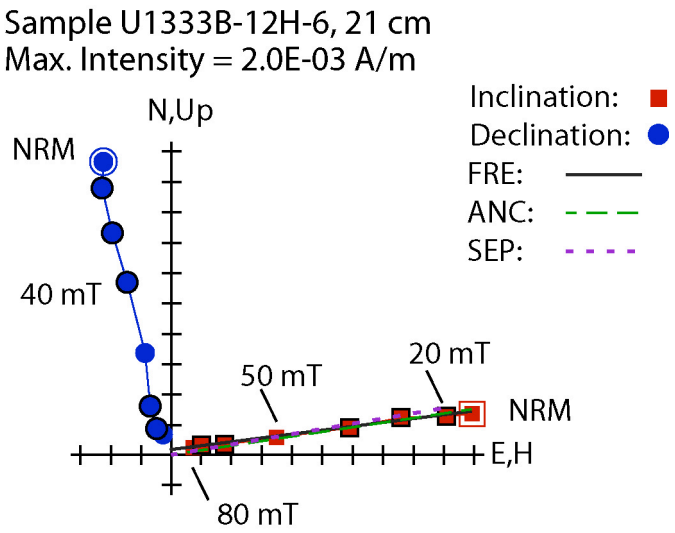

Figure S13. A typical vector demagnetization diagram for an interval along a U-channel sample. This particular U-channel was taken from an archive half core, which had been AF demagnetized at 20 mT during Expedition 320. That was sufficient to remove the low-coercivity drilling overprint common to IODP cores. The remaining magnetization decays to the origin illustrating the univectorial nature of the remanent magnetization. Lines fit through the data (shown only for the inclination) using the FREE and ANCHORED options of PCA and a Fisherian mean (SEP) are so similar that they plot on top of each other.

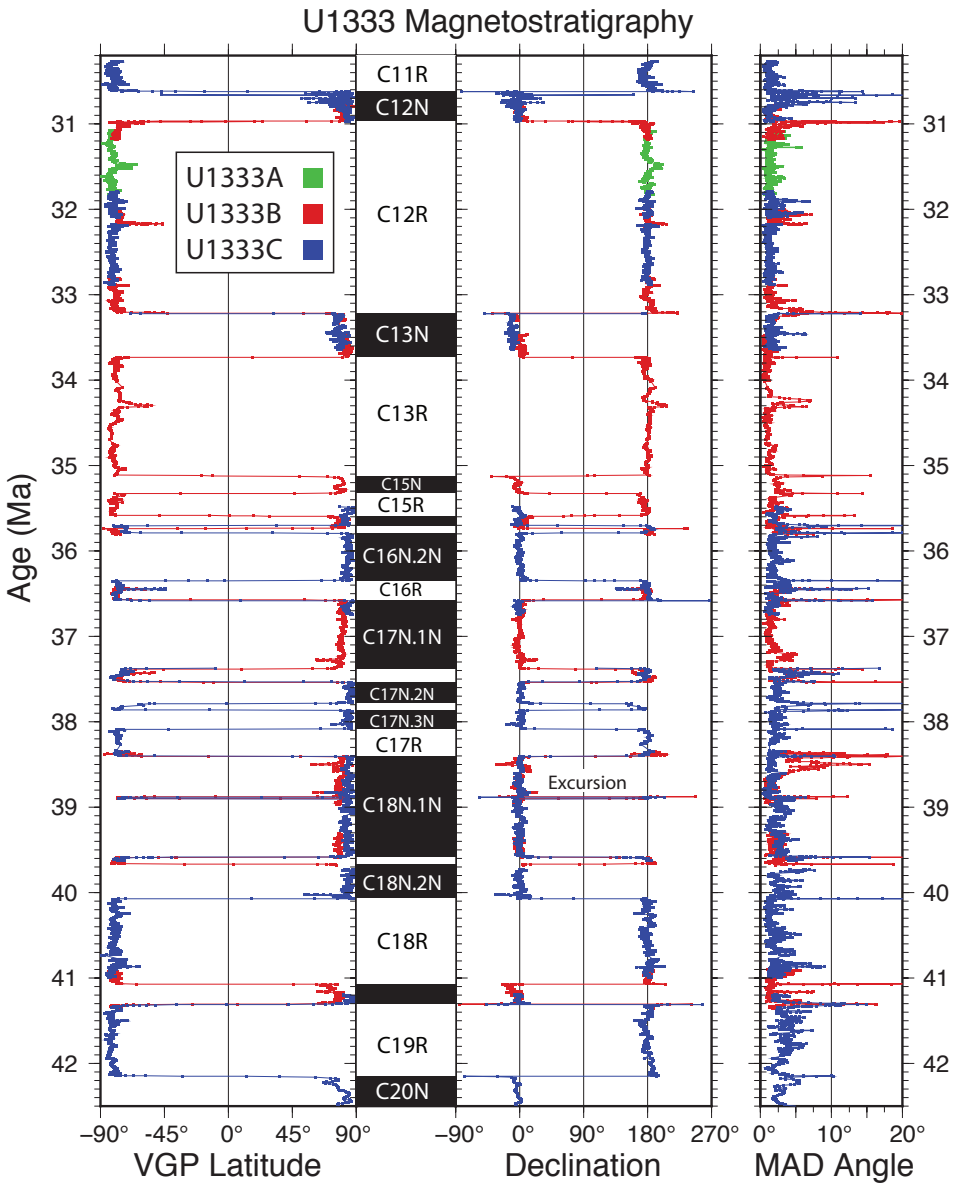

Figure S14. Magnetostratigraphy of Site U1333 from U-channel paleomagnetic data. The virtual geomagnetic pole (VGP) latitude, the declination, and the maximum angular deviation (MAD) angle from principal component analysis are plotted versus age. The average MAD angle is 2.3° and rarely does it exceed 7° except at reversal boundaries, which are associated with intervals when the geomagnetic field is weak and the geomagnetic direction more variable than within stable polarity intervals.

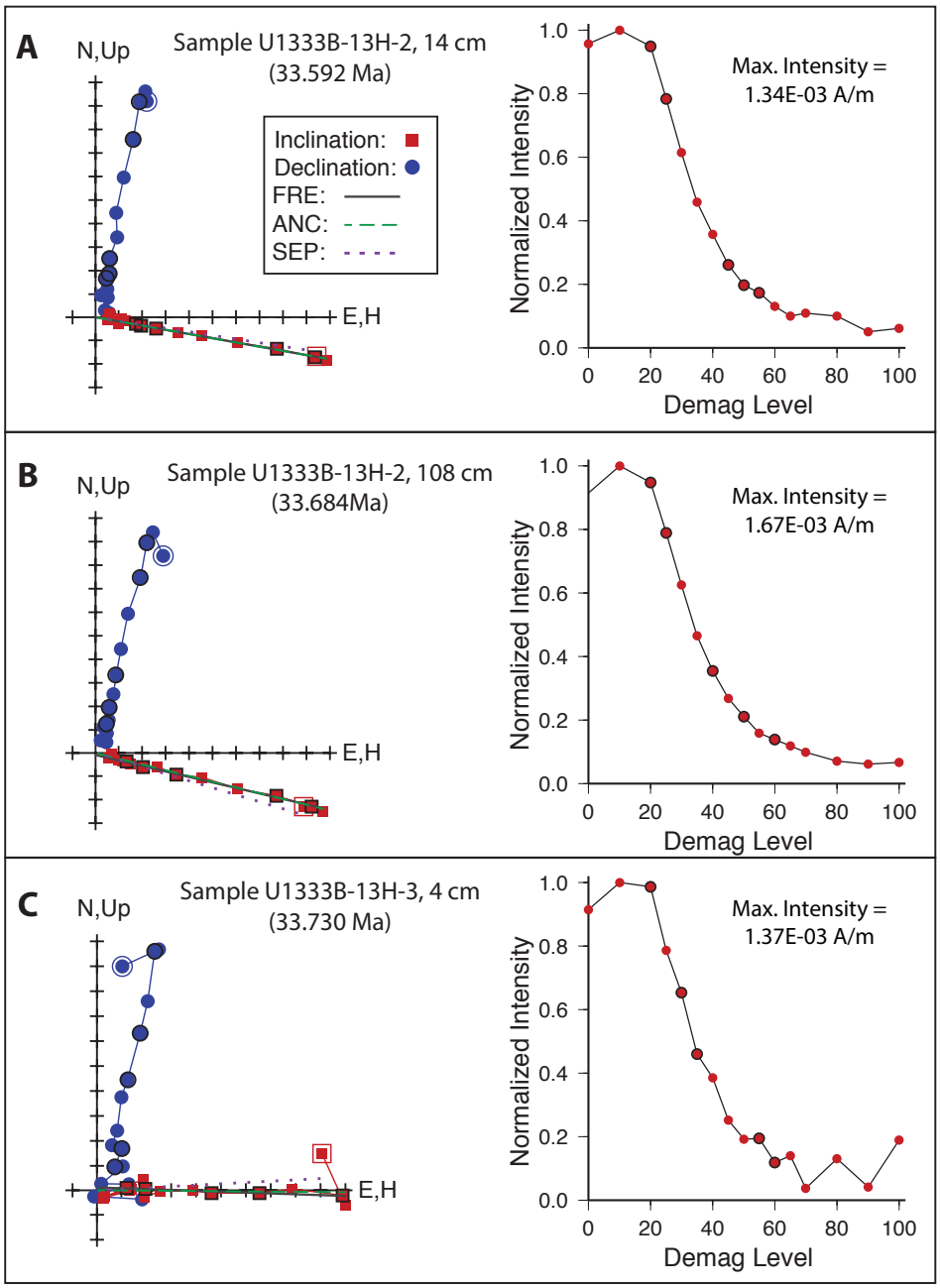

Figure S15a. Vector demagnetization diagrams and intensity decay plots for six intervals measured along U-channel samples that span the Chron C13n/C13r reversal. A) Sample U1333B-13H-2, 14 cm is a normal polarity sample 142 cm above the reversal, B) Sample U1333B-13H-2, 108 cm is a normal polarity sample 48 cm above the reversal, C) Sample U1333B-13H-3, 4 cm is a normal polarity sample 2 cm above the reversal, D) Sample U1333B-13H-3, 6 cm is a transitional sample in the very center of the Chron C13n/C13r reversal, E) Sample U1333B-13H-3, 9 cm is a reversed polarity sample 3 cm below the reversal, and F) Sample U1333B-13H-3, 90 cm is a reversed polarity sample 84 cm below the reversal.

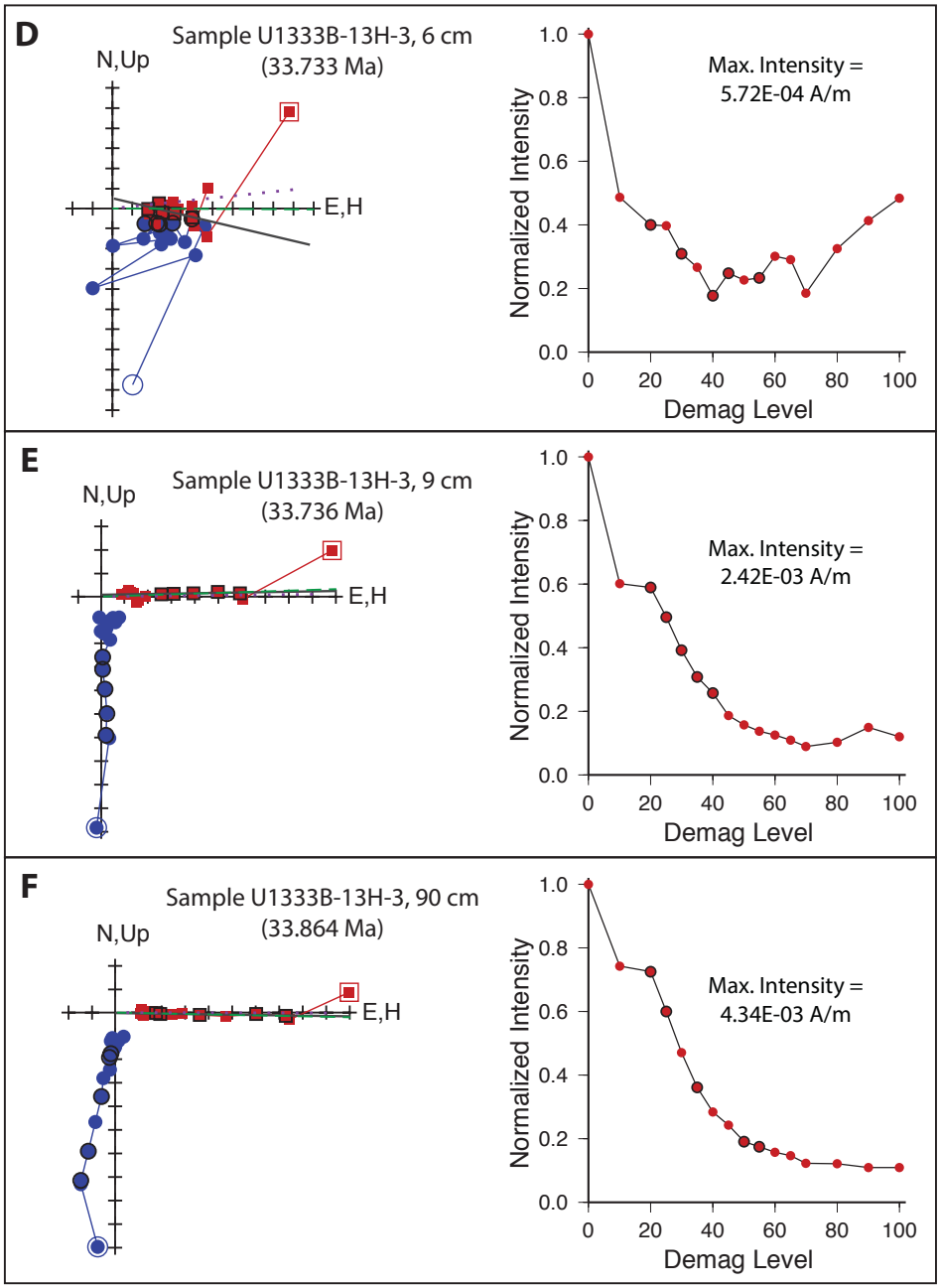

Figure S15b. – continued from pervious page.

Supplementary Material - Tables

The complete data set presented is available online in the WDC-MARE PANGAEA database at http://doi.pangaea.de/10.1594/PANGAEA.821903

Table S1. ODP Site 1218 XRF splice data

Table S2. ODP Site 1218A XRF raw data

Table S3. ODP Site 1218B XRF raw data

Table S4. ODP Site 1218C XRF raw data

Table S5. IODP Site U1333 XRF splice data

Table S6. IODP Site U1333A XRF raw data

Table S7. IODP Site U1333B XRF raw data

Table S8. IODP Site U1333C XRF raw data

Table S8. IODP Site U1334 XRF splice data

Table S10. IODP Site U1334A XRF raw data

Table S11. IODP Site U1334B XRF raw data

Table S12. IODP Site U1334C XRF raw data

Table S13. IODP Site U1333 bulk stable carbon isotope data

Table S14. IODP Site U1334 bulk stable carbon isotope data

Table S15. Astronomical tuned age model for Sites 1052, 1218, U1333 and U1334.

Table S16. Magnetostratigraphy and astronomically tuned ages of magnetochron boundaries of Sites 1218, U1333 and U1334.

Table S17. U1333A U-channel paleomagnetic data

Table S18. U1333B U-channel paleomagnetic data

Table S19. U1333C U-channel paleomagnetic data

References in supplementary

Bijl, P. K., A. J. P. Houben, S. Schouten, S. M. Bohaty, A. Sluijs, G.-J. Reichart, J. S. Sinninghe Damste, and H. Brinkhuis (2010), Transient Middle Eocene Atmospheric CO2 and Temperature Variations, Science, 330(6005), 819-821, 10.1126/science.1193654.

Bohaty, S. M., Zachos, J. C., Florindo, F., and Delaney, M. L.: Coupled greenhouse warming and deep-sea acidification in the middle Eocene, Paleoceanography, 24, 10.1029/2008pa001676, 2009.

Cande, S. C., and Kent, D. V.: Revised calibration of the geomagnetic polarity timescale for the Late Cretaceous and Cenozoic, Journal of Geophysical Research, 100, 6093-6095, 1995.

Coxall, H. K., Wilson, P. A., Pälike, H., Lear, C. H., and Backman, J.: Rapid stepwise onset of Antarctic glaciation and deeper calcite compensation in the Pacific Ocean, Nature, 433, 53-57, 10.1038/nature03135, 2005.

Coxall, H. K., and Wilson, P. A.: Early Oligocene glaciation and productivity in the eastern equatorial Pacific: Insights into global carbon cycling, Paleoceanography, 26, PA2221, 10.1029/2010pa002021, 2011.

Edgar, K. M., Wilson, P. A., Sexton, P. F., and Suganuma, Y.: No extreme bipolar glaciation during the main Eocene calcite compensation shift, Nature, 448, 908-911, 10.1038/nature06053, 2007.

Edgar, K. M., Wilson, P. A., Sexton, P. F., Gibbs, S. J., Roberts, A. P., and Norris, R. D.: New biostratigraphic, magnetostratigraphic and isotopic insights into the Middle Eocene Climatic Optimum in low latitudes, Palaeogeography, Palaeoclimatology, Palaeoecology, 297, 670-682, 10.1016/j.palaeo.2010.09.016, 2010.

Guidry, E. P., Richter, C., Acton, G. D., Channell, J. E. T., Evans, H. F., Ohneiser, C., Yamamoto, Y., and Yamazaki, T., 2013. Oligocene-Miocene magnetostratigraphy of deep-sea sediments from the Equatorial Pacific (IODP Site U1333), Geol. Soc. London, Spec. Pub., 373, 13-27, doi:10.1144/SP373.7.

Lanci, L., Pares, J.M., Channell, J.E.T., and Kent, D.V., 2004. Miocene magnetostratigraphy from Equatorial Pacific sediments (ODP Site 1218, Leg 199). Earth Planet. Sci. Lett., 226, 207-224.

Lanci, L., ParÈs, J.M., Channell, J.E.T., and Kent, D.V., 2005. Oligocene magnetostratigraphy from Equatorial Pacific sediments (ODP Sites 1218 and 1219, Leg 199). Earth Planet. Sci. Lett., 237, 617-634.

Laskar, J., Robutel, P., Joutel, F., Gastineau, M., Correia, A., and Levrard, B.: A long-term numerical solution for the insolation quantities of the Earth, Astronomy and Astrophysics, 428, 261-285, 10.1051/0004-6361:20041335, 2004.

Laskar, J., Fienga, A., Gastineau, M., and Manche, H.: La2010: a new orbital solution for the long-term motion of the Earth, Astronomy and Astrophysics, 532, A89, 10.1051/0004-6361/201116836, 2011a.

Laskar, J., Gastineau, M., Delisle, J. B., Farrés, A., and Fienga, A.: Strong chaos induced by close encounters with Ceres and Vesta, Astronomy and Astrophysics, 532, L4, 10.1051/0004-6361/201117504, 2011b.

Ogg, J. G., and Smith, A. G.: The geomagnetic polarity time scale, in: A Geological Timescale 2004, edited by: Gradstein, F., Ogg, J., and Smith, A., Cambridge University Press, 63-86, 2004.

Ogg, J. G.: Geomagnetic Polarity Time Scale, in: The Geological Timescale 2012, edited by: Gradstein, F., Ogg, J., Schmitz, M. D., and Ogg, G. M., Elsevier, 85-114, 2012.

Ohneiser, C., Acton, G., Channell, J.E.T., Wilson, G.S., Yamamoto, Y., and Yamazaki, T., 2013. A middle Miocene relative geomagnetic paleointensity record from the equatorial Pacific, Earth Planet. Sci. Lett., 374, 227-238, doi: dx.doi.org/10.1016/j.epsl.2013.04.038

Pälike, H., Moore, T., Backman, J., Raffi, I., Lanci, L., Parés, J. M., and Janecek, T.: Integrated stratigraphic correlation and improved composite depth scales for ODP Sites 1218 and 1219, in: Proc. ODP, Sci. Results, 199: College Station, TX (Ocean Drilling Program), edited by: Wilson, P. A., Lyle, M., and Firth, J. V., 1-41, 10.2973/odp.proc.sr.199.213.2005, 2005.

Pälike, H., Norris, R. D., Herrle, J. O., Wilson, P. A., Coxall, H. K., Lear, C. H., Shackleton, N. J., Tripati, A. K., and Wade, B. S.: The Heartbeat of the Oligocene Climate System, Science, 314, 1894-1898, 10.1126/science.1133822, 2006.

Pälike, H., Nishi, H., Lyle, M., Raffi, I., Gamage, K., Klaus, A., and the Expedition 320/321 Scientists: Proc. IODP, 320/321: Tokyo (Integrated Ocean Drilling Program Management International, Inc.), 2010.

Pares, J.M., and Lanci, L., 2004. A Middle Eocene – Early Eocene magnetic polarity stratigraphy in equatorial Pacific sediments. In: J.E.T. Channell, D.V. Kent, W. Lowrie, and J.G. Meert (Editors), Timescales of the Paleomagnetic Field. Amer. Geophysical Union, Washington DC, pp. 131-140.

Schulz, M., Berger, W. H., Sarnthein, M., and Grootes, P. M.: Amplitude variations of 1470-year climate oscillations during the last 100,000 years linked to fluctuations of continental ice mass, Geophysical Research Letters, 26, 3385-3388, 1999.

Shipboard Scientific Party: Site 1171, in: Proc. ODP, Init. Repts., 189: College Station, TX (Ocean Drilling Program), edited by: Exon, N. F., Kennett, J. P., Malone, M. J., and et al., 1-176, 10.2973/odp.proc.ir.189.106.2001, 2001.

Suganuma, Y., and Ogg, J. G.: Campanian through Eocene magnetostratigraphy of Sites 1257–1261, ODP Leg 207, Demerara Rise (western equatorial Atlantic), in: Proc. ODP, Sci. Results, 207: College Station, TX (Ocean Drilling Program), edited by: Mosher, D. C., Erbacher, J., and Malone, M. J., 1-48, 10.2973/odp.proc.sr.207.102.2006, 2006.

Wade, B. S., and Pälike, H.: Oligocene climate dynamics, Paleoceanography, 19, PA4019, 10.1029/2004PA001042, 2004.

Westerhold, T., Röhl, U., Wilkens, R., Pälike, H., Lyle, M., Jones, T. D., Bown, P., Moore, T., Kamikuri, S., Acton, G., Ohneiser, C., Yamamoto, Y., Richter, C., Fitch, P., Scher, H., Liebrand, D., and the Expedition 320/321 Scientists: Revised composite depth scales and integration of IODP Sites U1331-U1334 and ODP Sites 1218-1220, in: Proc. IODP, 320/321: Tokyo (Integrated Ocean Drilling Program Management International, Inc.), edited by: Pälike, H., Lyle, M., Nishi, H., Raffi, I., Gamage, K., Klaus, A., and the Expedition 320/321 Scientists, 10.2204/iodp.proc.320321.201.2012, 2012a.

Westerhold, T., Röhl, U., and Laskar, J.: Time scale controversy: Accurate orbital calibration of the early Paleogene, Geochem. Geophys. Geosyst., 13, Q06015, 10.1029/2012gc004096, 2012b.

Yamamoto, Y., Yamazaki, T., Acton, G., Richter, C., Guidry, E.P., and Ohneiser, C., 2013. Palaeomagnetic study of IODP Sites U1331 and U1332 in the equatorial Pacific—extending relative geomagnetic palaeointensity observations through the Oligocene and into the Eocene, Geophs. J. Int., doi: 10.1093/gji/ggt412.

Yamazaki, T, Yamamoto, Y., Acton, G., Guidry, E.P., and Richter, C., 2013. Rock-magnetic artifacts on long-term relative paleointensity changes in sediments, Geochem. Geophys. Geosyst., 14, 1-15, doi:10.1029/2012GC004546